Magnificent magpie colours by feathers with layers of hollow melanosomes

[1]Doekele G. Stavenga[*], [1]Hein L. Leertouwer, [2]Bodo D. Wilts

[1]Computational Physics, Zernike Institute for Advanced Materials, University of Groningen, NL-9747 AG Groningen, the Netherlands

[2]Adolphe Merkle Institute, University of Fribourg, Chemin des Verdiers 4, CH-1700 Fribourg, Switzerland

ORCID: DGS: 0000-0002-2518-6177 BDW: 0000-0002-2727-7128

Keywords: animal colouration – melanin – FDTD – thin films – iridescence

[*] **Correspondence**: D.G.Stavenga@rug.nl

Summary

The blue secondary and purple-to-green tail feathers of magpies are structurally coloured due to stacks of hollow, air-containing melanosomes embedded in the keratin matrix of the barbules. We investigated the feathers' spectral and spatial reflection characteristics by applying (micro)spectrophotometry and imaging scatterometry. To interpret the spectral data, we performed optical modelling, applying the Finite-Difference Time-Domain (FDTD) method as well as an effective media approach, treating the melanosome stacks as multilayers with effective refractive indices dependent on the component media. The differently coloured magpie feathers are realised by adjusting the melanosome size, with the diameter of the melanosomes as well as their hollowness being the most sensitive parameters that influence the appearance of the feathers.

Introduction

Many bird species feature brightly coloured plumage due to pigments and/or structural effects. The most common pigments of bird feathers are the carotenoids and melanins. Carotenoids strongly absorb in the blue to green wavelength range, thus causing yellow, orange or red feathers (McGraw, 2006a; Shawkey et al., 2009). The melanins, are deposited in small organelles, so-called melanosomes (McGraw, 2006b; Prum, 2006; Shawkey et al., 2009), which are usually irregularly organised and thus cause matte colours: eumelanin creates grey to black, and phaeomelanin causes rather brown and rufous colours (Hill, 2010). In the absence of pigments, the feathers are generally white, due to random scattering of incident light on the feathers' inhomogeneities (Prum, 2006; Leertouwer et al., 2011). However, feather barbs containing a quasi-regularly organised, spongy medullary keratin matrix display a distinct blue structural colour, which is turned into green when filtered by short-wavelength absorbing pigments (Prum, 2006; Shawkey et al., 2009; Stavenga et al., 2011; D'Alba et al., 2012; Tinbergen et al., 2013).

Some bird species feature shiny, structurally coloured feathers due to cuticular thin film effects, as is the case in for instance pigeons (Yoshioka et al., 2007), grackles (Shawkey et al., 2006) and crows (Lee et al., 2012). Strikingly, many bird species have structurally coloured feathers due to layers of orderly arranged melanin. The high density of melanin pigment in the melanosomes creates a high absorption coefficient throughout the visible wavelength range, resulting in a higher refractive index than that of the surrounding keratin. By arranging melanosomes in the feather barbules in more or less regular patterns with nanosized dimensions, vivid iridescent colours are created due to constructive interference in a restricted wavelength range (Durrer, 1977; Prum, 2006).

The melanosomes come in many different shapes and forms, and their spatial arrangement is similarly diverse (Prum, 2006). This has been shown in impressive detail by Durrer (Durrer, 1977), who performed extensive transmission electron microscopy of the feather barbules of numerous bird species. He already interpreted the observed structural colours to be created by regularly ordered melanosome stacks acting as optical multilayers. This view was fully confirmed for the male bird of paradise *Parotia lawesii*, which has bright-silvery occipital feathers because of widely spaced layers of melanin rodlets in the barbules. From measurements of the barbules' reflectance and transmittance spectra, while using the previously determined refractive index of keratin, the wavelength-dependent complex refractive index of melanin could be derived (Leertouwer et al., 2011; Stavenga et al., 2015).

The breast feathers of male *Parotia lawesii* have barbules that reflect strongly golden-orange, green or blue, depending on the angle of illumination and observation. The boomerang-shaped barbules contain densely packed stacks of solid melanosomes (Stavenga et al., 2010; Wilts et al., 2014). Using the measured melanin and keratin refractive index spectra, the various reflection phenomena could be well-explained by applying the finite-difference time-domain (FDTD) method, which is the method of choice for modelling the reflection and absorption properties of intricate, complex-shaped photonic structures (Wilts et al. 2014). Another exemplary case is that of the feather barbules of the male Common Bronzewing, *Phaps chalcoptera*, which have neatly arranged layers of solid melanin rodlets interleaved and separated by keratin. This spatial arrangement acts as an optical multilayer reflecting maximally blue, green, or red light, depending on the size and distance of the melanosomes. The measured reflectance spectra could be well explained by treating the melanosome stacks as optical multilayers and implementing the effective refractive index profiles of the barbules (Xiao et al., 2014). Instead of well-separated melanosome layers, the structural coloured feather barbules of mallards contain stacks of close-packed, solid melanin rodlets (Eliason and Shawkey, 2012; Khudiyev et al., 2014). Calculations with the FDTD method and multilayer modelling yielded virtually identical reflectance spectra, well corresponding to measured spectra (Stavenga et al. 2017).

Solid melanin rodlets embedded in a surrounding keratin matrix realise a refractive index (RI) contrast that is distinct but not impressive, with wavelength-dependent RI contrasts between 1.13-1.18. A much larger RI contrast of ~1.7-1.8 is realised in hollow melanosomes with an air core. In bird feathers, hollow melanosomes, structured as hollow cylinders or flattened balloons, cause the striking structural colours of the feather barbules of numerous bird species, e.g. trogonids (Durrer and Villiger, 1966), starlings and turkeys (Durrer and Villiger, 1967; Durrer and Villiger, 1970; Maia et al., 2013; Eliason et al., 2013). Notably the brightly coloured hummingbirds have excessively large stacks of hollowed melanosomes in their feather barbules (Greenewalt et al., 1960; Durrer, 1977; Osorio and Ham, 2002; Parra, 2010; Meadows et al., 2011).

Hollow melanosomes are also found in the barbules of the blue secondaries and the variably coloured tail feathers of the Eurasian or common magpie, *Pica pica*. The melanosomes are cylindrical rodlets, close-packed and pressed against the barbule's epicuticle in a few layers, causing a distinct, iridescent colouration. To explain the magpie feathers' reflectance spectra, the lattice of air holes that form the core of the melanosomes has been presumed to act as a

colour-creating grating (Vigneron et al., 2006). In a related study, on the black-billed magpie, *Pica hudsonia*, the stack of about hexagonally packed, hollow melanosomes was treated as a two-dimensional photonic crystal, using photonic bandgap theory, taking into account the rodlet dimensions as well as the refractive indices of the material components of the barbules, keratin, melanin and air (Han et al., 2017). Close examination of the cross-sectional microstructures of the magpie feather barbules revealed, however, that the lateral arrangement was of minor importance and that the vertically layered structure of melanin rodlets along the barbule surface is responsible for the iridescence (Han et al., 2017).

Here we revisit the colouration of common magpie feathers by comparing finite-difference time-domain (FDTD) simulations with effective-medium multilayer (EMM) modelling. Treating the melanosome stacks as gradient multilayers, we find that multilayer optics allows ready understanding of the colouration of magpie feathers, thus expanding our insight into the intricacies of bird feather colouration.

Materials and Methods

Specimens

Common magpie feathers were collected in a local park in Groningen, NL, and purchased from a commercial supplier (Etsy, UK). Light microscopic images of the feather barbules were taken with a Zeiss Universal Microscope (Zeiss, Oberkochen, Germany).

Electron Microscopy

The barbule anatomy was investigated by transmission electron microscopy (TEM) using standard methods. Briefly, a feather piece was, after a dehydration series, embedded in resin, and sections were stained using 2% aqueous uranyl-acetate solution and examined with a Hitachi 7100 TEM. Additionally, for scanning electron microscopy, barbules were sputtered with a 3 nm thick layer of gold and observed with a MIRA 3 LMH field-emission electron microscope (Tescan, Brno, Czech Republic).

Spectroscopy

Reflectance spectra of different feather areas were measured with an integrating sphere (AvaSphere-50), using an AvaSpec 2048-2 CCD detector array spectrometer (Avantes, Apeldoorn, Netherlands). The light source was a deuterium-halogen lamp (AvaLight-D(H)-S), and the reference was a white diffuse reflectance tile (Avantes WS-2). The angle- and polarisation-dependence of the reflectance spectra of the feathers was measured by using two

optical fibres. One end of the first optical fibre was connected to a xenon lamp, and its other end was mounted at a goniometer together with a small lens, which focused the fibre tip at the goniometer's rotation axis. At a second goniometer one end of the second fibre was mounted with a focusing lens and a rotatable polarisation filter, and the other end of the fibre was connected to the CCD detector array spectrometer. The rotation axes of the two goniometers coincided and the two fibres rotated in about the same plane. The area to be measured was positioned in that plane, at the axis of rotation of the goniometers. The aperture of the fibres was 5º (full width at half maximum, FWHM) and the distance of the tips to the centre of the illuminated spot was 6 and 12 cm, respectively. The receiving fibre thus sampled a larger area than the illuminated spot but captured only a small part of the reflected light. The white diffuse reflectance tile (Avantes WS-2) served as reference. Reflectance spectra of isolated barbules attached to the tip of a glass micropipette were measured with a microspectrophotometer (MSP), which consisted of a Leitz Ortholux microscope (Leitz, Wetzlar, Germany) connected to the detector array spectrometer, with as light source a xenon arc lamp. Transmittance spectra of isolated barbules, immersed in immersion oil (refractive index 1.515), were also measured with the MSP; the measured area was a square with edge length 5-10 µm. The microscope objective was an Olympus 20x, NA 0.46 (Olympus, Tokyo, Japan). Due to the glass optics, the MSP spectra were limited to wavelengths >350 nm.

Imaging scatterometry

For investigating the spatial reflection characteristics of the barbules, we performed imaging scatterometry (Stavenga et al., 2009; Vukusic and Stavenga, 2009; Wilts et al., 2009). A small feather piece attached to a glass micropipette was positioned at the first focal point of the ellipsoidal mirror of the imaging scatterometer. The scatterograms were obtained by focusing a white light beam with a narrow aperture (< 5º) onto at a small circular area, and the spatial distribution of the far-field scattered light was then monitored. A flake of magnesium oxide served as a white diffuse reference object.

Modelling

Using parameter values inspired by anatomy, we calculated the reflectance, transmittance and absorptance of model magpie barbules using Lumerical FDTD solutions 8.16, a commercial-grade Maxwell equation solver. Being based on fundamental Maxwell theory, the FDTD method enables the detailed simulation of the light flux in any complex-structured material with arbitrary refractive index and spatial arrangement. Simulations were performed in a volume of

~3x3x5 μm^3. The model barbules contained two stacks of melanosomes, each near the two opposite sides of the barbule, embedded in a keratin matrix. As the refractive index of a material is generally complex, $\tilde{n} = n - ik$, the real parts of the wavelength-dependent refractive indices of keratin and melanin, n_k and n_m, were calculated with the Cauchy formula $n = A + B\lambda^{-2}$ (λ is the light wavelength), using for keratin A_k = 1.532 and B_k = 5890 nm^{-2} and for melanin A_m = 1.648 and B_m = 23700 nm^{-2}; the imaginary component of the refractive index of keratin was assumed to be negligible in the wavelength of interest, but that of melanin was taken to be $k_m = a_m \exp(-\lambda/b_m)$, with a_m = 0.56 and b_m = 270 nm (Leertouwer et al., 2011; Stavenga et al., 2015; the refractive index of the air core was n_a = 1). We compared the FDTD results with effective-medium multilayer modelling (EMM) performed with a transfer-matrix program based on classical optical multilayer theory, written in Matlab (Stavenga, 2014). We therefore sliced the melanosome stacks into 10 nm thin layers and calculated the volume fractions of the components keratin, melanin, and air, f_k, f_m, and f_a, of each layer, with $f_k + f_m + f_a = 1$. The effective refractive index of each 10 nm layer was then calculated with the volume fractions of the components:

$$\tilde{n}_{eff} = (f_k n_k^w + f_m \tilde{n}_m^w + f_a n_a^w)^{1/w} \quad (1)$$

For light incident on a layer of parallel rods, effective medium theory predicts for light polarised perpendicular to the rods a weighting factor w = -2, and for light polarised parallel to the rods w = 2 (Bräuer and Bryngdahl, 1994; Lucarini et al., 2005; Halir et al., 2015). We also investigated the cases with w = -1 and 1.

Results

Colours and anatomy of magpie feathers

The common magpie, *Pica pica*, has blue secondaries and tail feathers with a distinct colour gradient, shifting from green (proximal) via purple to blue (distal; Fig. 1). Reflectance spectra measured from different areas of a secondary feather show slightly varying, broad reflectance bands in the blue wavelength range (Fig. 1B), and the reflectance spectra measured along the length of a tail feather gradually shift along the wavelength scale (Fig. 1C).

The reflectance spectra confirmed the structural basis of the feather colours. We therefore also investigated the spatial reflection properties of the barbules. Microscopic inspection of isolated feather barbs (with barbules) showed that most parts of the barbules are black, clearly due to the abundant presence of irregularly distributed melanin; these parts are overlapped by the exposed coloured parts of adjacent barbules *in situ* (Fig. 2A-C). Studying the coloured barbules with an imaging scatterometer showed that illumination of a small feather with a small

aperture, white-light beam resulted in light reflected into a narrow spatial wedge, oriented about perpendicular to the barbule's long axis (Fig. 2D-E). Closer inspection showed that the barbules are rows of elongated cells. The colour of the cells strongly depends on the location in the feather; it can slightly differ between neighbouring cells, and even can distinctly vary within each cell (Fig. 2G-I).

To study the colouration in more detail, we performed high-magnification epi-illumination light microscopy as well as electron microscopy. This revealed that the barbule colouration emerges from tightly-packed, sub-micrometer-sized particles: the melanosomes. Epi-illumination of a green area of a tail feather immersed in oil revealed that the barbules contain slightly disordered, blue-to-yellow coloured rod-like particles (Fig. 3A). Transmitted light microscopy showed a completely different, red-brown colour, the signature of melanin. An ellipsoid-shaped area in each cell indicated the remnant of the cell nucleus (Fig. 3B). Similar to the elongated particles observed by light microscopy, scanning electron microscopy of intact barbules showed tightly-organised small rodlets, length 1-2 µm and width ~0.2 µm (Fig. 3C). Cross-sectioning the barbules demonstrated that the melanosomes are assembled into two stacks onto both sides of the barbule and that the rodlets are hollow, pressed against the cell surface in 2-4 layers (Fig. 3D-F). Transmission electron microscopy showed that the melanosome diameter varied between 160 and 200 nm, and that the air core diameter varied between 90 and 110 nm (Fig. 3E).

Microspectrophotometry of magpie barbules

To ascertain that the coloured barbules contain melanin, we measured absorbance spectra of single barbules immersed in oil (refractive index 1.515) with a microspectrophotometer, which clearly demonstrated that the absorbance is dominated by melanin absorption (Fig. S1A). Reflectance spectra measured from small areas (diameter ~4 µm) of barbules (in air) taken from various tail feather locations showed marked high-frequency oscillations in the long-wavelength range, clearly indicating thin-film-like light interference (Fig. S1B). Analysing the oscillations as established before (Stavenga, 2014) and by assuming an effective refractive index of the barbule of ~1.6, yielded barbule thicknesses of 2.0–3.5 µm (Fig. S1C), in full accordance with the barbule thickness following from anatomy (Fig. 3E,F). When measuring reflectance spectra from areas exceeding a diameter of ~20 µm, the oscillations vanished, evidently because integration of the reflectance of larger areas causes smoothing of the local variations (Fig. 1B,C).

Modelling magpie barbule optics

Based on the anatomical data, we performed optical modelling by considering a 3 µm thick barbule, with on both sides N = 3 melanosome layers, surrounded by an epicuticle with thickness t_c = 50 nm. The close-packed, cylindrical melanosomes were assumed to have an air core with diameter d_a = 100 nm, and a melanin cladding with diameter d_m = 180 nm (Fig. 4, middle inset). We calculated the reflectance spectra for normally incident light, polarised parallel (TE) and perpendicular (TM) to the melanosome axes (Fig. 4, upper inset), applying the FDTD method (Fig. 5A).

The reflectance spectra for TE- as well as TM-polarised light showed high frequency oscillations (Fig. 5A, full), evidently due to thin-film interference of the total barbule thickness. To confirm this, we also calculated the reflectance spectra for half the barbule (bounded by the dashed vertical line in Fig. 4, middle inset). The resulting TE- and TM-spectra no longer featured the oscillations and only had a main, broad reflectance band, peaking at ~500 nm. Interestingly, the latter spectra are almost identical to the smoothed spectra of the full model barbule. In other words, the reflectance is almost completely determined by the upper melanosome stack.

Simultaneous with the reflectance, we also calculated the transmittance of both the full and half barbule for TE- and TM-polarised light, which yielded the absorptance (the absorptance is 1 minus the sum of the reflectance and transmittance). The absorptance spectra clearly show the strong wavelength-dependent absorption of melanin that monotonically decreases for long wavelengths (Fig. 5B). Additionally, a reduced absorptance is visible at the position of the reflectance peak. The absorptances of the full and half barbule only slightly differ, indicating that the upper melanosome stack absorbs the main part of the incident light, leaving only a small part of the light flux to be additionally absorbed by the lower stack.

Dependence of the reflectance on the number of melanosome layers and melanosome hollowness

We subsequently investigated the consequences of changes in the number of melanosome layers, N, while keeping the melanosome outer diameter d_m = 180 nm and the inner diameter d_a = 100 nm fixed. The reflectance spectra, calculated with the FDTD method, exhibit two major effects: (*i*) With an increasing number of melanosome layers the reflectance rapidly increases and the bandwidth narrows, saturating when $N > 5$ (Fig. 6A,B); (*ii*) The reflectance spectra show oscillations that increase in frequency with the number of melanosome layers, or, increase

proportional to the thickness of the internal melanosome stack, which also will act as a thin film interference reflector.

Changing the hollowness of the melanosomes, $h = d_m/d_a$, has quite different optical effects. Keeping the melanosome outer diameter d_m = 180 nm and the number of layers N = 3 fixed, an increasing air core diameter d_a (larger hollowness) yields a gradually rising reflectance until $d_a \approx 150$ nm (Fig. 6C,D). The reflectance spectra have a clear, main band for $60 < d_a < 100$ nm, but for $d_a > 100$ nm the spectra become progressively bimodal. A prominent single reflectance band is realised when $d_a \approx 90$, or, $h \approx 0.5$ (Fig. 6C,D).

The magpie feather barbule considered as a multilayer reflector

The prominent optical feature revealed by the FDTD calculations is a strong polarisation-dependency of the feathers as TE-polarised light has a significantly higher reflectance compared to TM-polarised light (Figs. 5, 6). This optical anisotropy must be intimately related to the shape anisotropy of the melanosome stacks, being assemblies of parallel cylindrical rodlets (Figs. 3, 4). We therefore considered the refractive index profile of the melanosome stack. We sliced the model barbule of Figure 4 into 10 nm layers and calculated the fractions of air, keratin and melanin as a function of depth into the barbule for melanosomes of different hollowness (Fig. S2). The effective refractive index of each layer was then obtained by using Eq. 1 (Methods). The weighting factors for TE- and TM-polarised light, w = -2 and 2, yielded a much larger refractive index contrast for TE- than for TM-polarised light (Fig. 4). Subsequently we performed effective-medium multilayer modelling (EMM) by applying a standard transfer-matrix formalism for optical multilayers to calculate the reflectance, transmittance and absorptance for both the full and half barbule. The resulting spectra are remarkably similar to those obtained with the FDTD simulations (compare Fig. S3 with Fig. 5). The reflectance of TE-polarised light is much larger than that of TM-polarised light, evidently due to the larger refractive index contrast of the layers for TE-light.

We also performed transfer-matrix calculations for the same parameter set as used in the FDTD modelling of Fig. 6. The resulting reflectance spectra (Fig. S4) are again very similar to those obtained with the FDTD approach. Figure 7 compares the peak reflectance, peak wavelength, and bandwidth (FWHM) of the spectra obtained with the FDTD method and the EMM results for four cases, using as weighting factors for the effective refractive index of the layers w = -2, -1, 1, and 2. Figs. 7A-C present the results for varying numbers of melanosome layers, and Figs. 7D-F show the results for different melanosome hollowness with a fixed number of layers. The overall behaviour of the FDTD and EMM spectra are clearly very similar,

but the differences demonstrate that the heuristic expression for the effective refractive index with the chosen values of the weighting factor *w* is not fully adequate. The FDTD and EMM approach give approximately the same results for TE- and TM-polarised light when choosing *w*-values of ~-0.5 (TE) and ~2.5 (TM), respectively.

Because the multilayer modelling facilitates an intuitive interpretation of the optical properties of magpie barbules, we applied this approach in a study of the effect of melanosome size. We calculated the reflectance spectra of a half barbule with three layers of melanosomes that are close packed for normally incident light. The melanosomes are assumed to have a constant hollowness $h = 0.5$, but with a changing melanosome diameter, from 140 to 220 nm (Fig. 8A). Weighting factors $w = -0.5$ (TE) and $w = 2.5$ (TM) for the effective refractive index of the layers yielded strongly different reflectance spectra for TE- and TM-polarised light. The increase in melanosome size causes a distinct shift in peak wavelength, from ~400 nm to ~600 nm, an increase of the peak reflectance, and a broadening bandwidth. Averaging the TE- and TM-spectra yielded the reflectance for unpolarised light (Fig. 8A, av).

The reflectance spectra calculated for normally incident TE- and TM-polarised light are substantially different in amplitude and also in peak wavelength. Measurements of the polarisation-dependent reflectance spectra from different locations on the tail feather of Fig. 1C confirm the severe dependence on polarisation and thus the distinct optical effects of the anisotropy of the melanosome stacks (Fig. 8B).

We finally studied the dependence of the reflectance spectra for TE- and TM-polarised light on the angle of incidence. The peak reflectance of the TE-spectra increases monotonically with an increasing angle of incidence while the peak reflectance of the TM-spectra decreases up to the Brewster angle, fully in accordance with the reflection behaviour of isotropic multilayers (Fig. S5).

Discussion

Optical properties of magpie feathers

Our study compares measured reflectance spectra of magpie barbules with the results of modelling with the FDTD method and classical multilayer modelling using effective medium theory. In the magpie feathers, the coloured barbules approximate slightly-bent thin plates, and thus in principle they will act as optical thin films. In general practice, however, the varying barbule thickness will obscure the thin film interference effects due to spectral smoothing (Figs. 1, S1).

The barbules contain hollow melanosomes, which are closely packed into a few layers and organised into two stacks, each of which is located on the outer edges of the barbules. The feather brightness is proportional to the number of melanosome layers, and the colour crucially depends on the melanosome diameter and hollowness (Figs. 6, 7). Calculations of the reflectance as a function of the number of layers demonstrated that it is hardly useful to install more than 3 or 4 melanosome layers to achieve magnificent feather colours. Optical modelling further established that the first reflector stack is virtually exclusively responsible for the observed coloration. Why the barbules nevertheless have two stacks, located at the outer edges of the cells, may likely be the consequence of the cellular process of pulling the melanosomes together against the cell wall during the feather's development, before the barbule cell dies (as e.g. discussed in Shawkey et al., 2015).

Recent TEM studies on black-billed magpie feathers revealed that the number of melanosome layers locally vary, corresponding with the local colour (Han et al., 2017). Furthermore, both optical and anatomical data indicated that the size and arrangement of the melanosomes is too irregular to treat the melanosome stack as an ideal photonic crystal (Figs. 2,3; Han et al., 2017). In our modelling we nevertheless used a regular melanosome packing in order to derive the refractive index profile (Fig. 4,5), applying an effective medium approach. The reflectance spectra thus obtained compared well with the spectra following from FDTD modelling. In real barbules, a much shallower refractive index profile than those used in the modelling can occur, indicating that the reflectance is strongly dependent on the degree of irregularity of the spatial arrangement of the melanosomes. This will however not seriously affect the wavelength range of the reflectance spectra, but it will reduce their magnitude (for a related analysis of the effect of melanosome disorder in mallard barbules see Stavenga et al., 2017). The experimentally obtained reflectance spectra (Fig. 1, 8B) have a distinctly lower amplitude than the modelled ones (Figs. 5, 6, 8A), which is because of the spatial spread of the reflected light and hence mostly due to the experimental conditions. The measured spectra noticeably differ from the modelled spectra in the long-wavelength range. The latter will be the result from light scattering in the lower feather parts, because melanin absorption rapidly decreases with increasing wavelength, and thus long-wavelength scattered light will be progressively less absorbed by the melanin of the feathers, resulting in a rising reflectance with increasing wavelength (e.g. Fig. S3), which however occurs beyond the spectral range of the bird's vision.

Barbule anisotropy and dependence of the reflectance on polarisation

FDTD calculations as well as multilayer-modelling indicated that the shape of the melanosomes and their spatial arrangement causes a distinct shape anisotropy of the barbule and thus a clear polarization-dependence of the reflectance spectra, which was confirmed experimentally (Fig. 8). The polarised reflections of the feathers are presumably not functional however, because birds are not known to possess polarization vision. The feather colours as seen by a conspecific will hence be the result of averaged TE- and TM-reflectance. Only with very large angles of light incidence, this will cause an iridescent signal. Whether magpies use iridescence in intraspecific recognition is doubtful, especially as the tail feathers have a rather varied colouration, although magpies will most likely have acute colour vision (Lind et al., 2013). Whether the black feathers, having strongly absorbing melanin, and the white feathers, where melanin is absent, increase or decrease the risk of attack of magpies by goshawks has been studied (Götmark, 1997), but the general biological functions of the pigmentary and structural colouration of the magpie plumage has so far remained uncharted territory.

Colouration of other magpies and related corvids

The plumage of magpies (Corvidae) does not have a universal colouration mechanism. Whereas the feathers of the closely related Korean magpie, *Pica sericea*, have barbules with hollow melanosomes similar as the Eurasian magpie investigated here (Lee et al., 2010), the Formosan (or Taiwan) blue magpie, *Urocissa caerulea*, derives its blue colouration from light interference in the spongy medulla of the feather barbs (Liao et al., 2015). Similarly, the structural colouration of the Common Green Magpie, *Cissa chinensis*, is also based in the barbs, but the observed green colour arises from a filtering action of frontally deposited carotenoids. *C. chinensis* is green when in forest area, but becomes blue when in open country or when reared on a low carotenoid diet (Rothschild, 1975; Hudon, 2005). Remarkably the same optical method is realised in the green feathers of budgerigars and parrots, but here the high-pass colour filters are psittacofulvins (McGraw and Nogare, 2004; D'Alba et al., 2012; Tinbergen et al., 2013).

Magpies thus apply a diversity of colouration methods, as is generally the case with other corvids (Lee et al., 2016). In addition to thin film reflections causing the shiny appearance of many crows, the two main ways of structural colouration are regularly ordered melanosomes in the barbules and a quasi-regular ordered spongy medulla in the barbs. The melanosomes can be solid or hollow (Durrer, 1977; Prum, 2006); intermediate states with a dense melanised cladding and a less dense core also exist, e.g. in the occipital feather melanosomes of *Parotia lawesii*

(Stavenga et al., 2015). Another colourful corvid is the blue jay, which has blue and white feathers due to barbs with a spongy medulla ordered with different length scales, while rufous and black feathers are due to phaeomelanin and eumelanin (Parnell et al., 2015). Similar to the polarisation signals discussed above, the physico-chemical basis of the feather colours of many corvids and its connection to vision remains largely uninvestigated, a gap that future studies might close.

Acknowledgments

We thank Dr Julian Thorpe (University of Sussex, UK) for performing transmission electron microscopy and Dr Daniel Osorio for advice and reading the manuscript.

Competing interests.

The authors declare no competing or financial interests.

Author contributions.

Study design: DGS, BDW; performed measurements: DGS, HLL, BDW; analysed measurements: DGS, BDW; performed modelling: DGS, BDW; wrote the manuscript: DGS, BDW; all authors gave final approval for publication.

Funding.

This study was financially supported by the Air Force Office of Scientific Research/European Office of Aerospace Research and Development AFOSR/EOARD (grant FA9550-15-1-0068, to D.G.S.) and the National Centre of Competence in Research “Bio-Inspired Materials”, the Adolphe Merkle Foundation, and the Ambizione program of the Swiss National Science Foundation (168223, to B.D.W.).

References

Bräuer, R. and Bryngdahl, O. (1994). Design of antireflection gratings with approximate and rigorous methods. *Appl. Opt.* **33,** 7875-7882.

D'Alba, L., Kieffer, L. and Shawkey, M. D. (2012). Relative contributions of pigments and biophotonic nanostructures to natural color production: a case study in budgerigar (*Melopsittacus undulatus*) feathers. *J. Exp. Biol.* **215,** 1272-1277.

Durrer, H. and Villiger, W. (1970). Schillerfarben der Stare (Sturnidae). *J.Ornithol.* **111,** 133-153.

Durrer, H. and Villiger, W. (1966). Schillerfarben der Trogoniden. *J.Ornithol.* **107,** 1-26.

Durrer, H. and Villiger, W. (1967). Bildung der Schillerstruktur beim Glanzstar. *Zeitschr. Zellforsch. Mikrosk. Anat.* **81,** 445-456.

Durrer, H. (1977). Schillerfarben der Vogelfeder als Evolutionsproblem. *Denkschr. Schweiz. Naturforsch. Ges.* **91,** 1-126.

Eliason, C. M., Bitton, P. P. and Shawkey, M. D. (2013). How hollow melanosomes affect iridescent colour production in birds. *Proc. R. Soc. B* **280,** 20131505.

Eliason, C. M. and Shawkey, M. D. (2012). A photonic heterostructure produces diverse iridescent colours in duck wing patches. *J. R. Soc. Interface* **9,** 2279-2289.

Götmark, F. (1997). Bright plumage in the magpie: does it increase or reduce the risk of predation? *Behav. Ecol. Sociobiol.* **40,** 41-49.

Greenewalt, C. H., Brandt, W. and Friel, D. D. (1960). The iridescent colors of hummingbird feathers. *Proc. Amer. Phil. Soc.* **104,** 249-253.

Halir, R., Bock, P. J., Cheben, P., Ortega-Moñux, A., Alonso-Ramos, C., Schmid, J. H., Lapointe, J., Xu, D., Wangüemert-Pérez, J. G. and Molina-Fernández, Í. (2015). Waveguide sub-wavelength structures: a review of principles and applications. *Laser Phot. Rev.* **9,** 25-49.

Han, C., Kim, H., Jung, H., Lee, S., Jablonski, P. G. and Jeon, H. (2017). Origin and biomimicry of weak iridescence in black-billed magpie feathers. *Optica* **4,** 464-467.

Hill, G. E. (2010). *Bird Coloration*. Washington: National Geographic.

Hudon, J. (2005). Considerations in the conservation of feathers and hair, particularly their pigments. In: *Proceedings of the CAC/ACCR 31st Annual Conference, Jasper, AB, Canada*. p. 127-147.

Khudiyev, T., Dogan, T. and Bayindir, M. (2014). Biomimicry of multifunctional nanostructures in the neck feathers of mallard (*Anas platyrhynchos* L.) drakes. *Sci. Rep.* **4,** 4718.

Lee, E., Lee, H., Kimura, J. and Sugita, S. (2010). Feather microstructure of the Black-billed Magpie (*Pica pica sericea*) and Jungle Crow (*Corvus macrorhynchos*). *J. Vet. Med. Sci.* **72,** 1047-1050.

Lee, E., Miyazaki, J., Yoshioka, S., Lee, H. and Sugita, S. (2012). The weak iridescent feather color in the Jungle Crow *Corvus macrorhynchos*. *Ornith. Sci.* **11,** 59-64.

Lee, S., Kim, M., Choe, J. C. and Jablonski, P. G. (2016). Evolution of plumage coloration in the crow family (Corvidae) with a focus on the color-producing microstructures in the feathers: a comparison of eight species. *Anim. Cells Syst.* **20,** 95-102.

Leertouwer, H. L., Wilts, B. D. and Stavenga, D. G. (2011). Refractive index and dispersion of butterfly scale chitin and bird feather keratin measured by interference microscopy. *Opt. Exp.* **19,** 24061-24066.

Liao, S., Yao, C. and Lee, C. (2015). Measuring and modeling the inconspicuous iridescence of Formosan blue magpie's feather (Urocissacaerulea). *Appl. Opt.* **54,** 4979-4983.

Lind, O., Mitkus, M., Olsson, P. and Kelber, A. (2013). Ultraviolet vision in birds: the importance of transparent eye media. *Proc. R. Soc. B* **281,** 20132209.

Lucarini, V., Saarinen, J. J., Peiponen, K. and Vartiainen, E. M. (2005). *Kramers-Kronig relations in optical materials research*: Springer: Berlin.

Maia, R., Rubenstein, D. R. and Shawkey, M. D. (2013). Key ornamental innovations facilitate diversification in an avian radiation. *Proc. Natl. Acad. Sci. U. S. A.* **110,** 10687-10692.

McGraw, K. J. (2006a). Mechanics of carotenoid-based coloration. In *Bird Coloration, Vol. 1* (ed. G. E. Hill and K. J. McGraw), pp. 177-242. Cambridge, Ma: Harvard.

McGraw, K. J. (2006b). Mechanics of melanin-based coloration. In *Bird Coloration, Vol. 1* (ed. G. E. Hill and K. J. McGraw), pp. 243-294. Cambridge, Ma: Harvard.

McGraw, K. and Nogare, M. (2004). Carotenoid pigments and the selectivity of psittacofulvin-based coloration systems in parrots. *Comp. Biochem. Physiol. B* **138,** 229-233.

Meadows, M. G., Morehouse, N. I., Rutowski, R. L., Douglas, J. M. and McGraw, K. J. (2011). Quantifying iridescent coloration in animals: a method for improving repeatability. *Behav. Ecol. Sociobiol.* **65,** 1317-1327.

Osorio, D. and Ham, A. D. (2002). Spectral reflectance and directional properties of structural coloration in bird plumage. *J. Exp. Biol.* **205,** 2017-2027.

Parnell, A. J., Washington, A. L., Mykhaylyk, O. O., Hill, C. J., Bianco, A., Burg, S. L., Dennison, A. J., Snape, M., Cadby, A. J. , Smith, A., Prevost, S., Whittaker, D. M. Jones, R. A. L., Fairclough, J. P. A. and Parker, A. R. (2015). Spatially modulated structural colour in bird feathers. *Sci. Rep.* **5,** 18317

Parra, J. L. (2010). Color evolution in the hummingbird genus *Coeligena*. *Evolution* **64,** 324-335.

Prum, R. O. (2006). Anatomy, physics, and evolution of avian structural colors. In *Bird Coloration, Vol. I, Mechanisms and Measurements* (ed. G. E. Hill and K. J. McGraw), pp. 295-353. Cambridge, Mass.: Harvard University Press.

Rothschild, M. (1975). Remarks on carotenoids in the evolution of signals. In *Coevolution of animals and plants* (ed. L.E. Gilbert, P H Raven), pp. 20-52: University of Texas Press, Austin.

Shawkey, M. D., D'Alba, L., Xiao, M., Schutte, M. and Buchholz, R. (2015). Ontogeny of an iridescent nanostructure composed of hollow melanosomes. *J. Morphol.* **276,** 378-384.

Shawkey, M. D., Hauber, M. E., Estep, L. K. and Hill, G. E. (2006). Evolutionary transitions and mechanisms of matte and iridescent plumage coloration in grackles and allies (Icteridae). *J. R. Soc. Interface* **3,** 777-786.

Shawkey, M. D., Morehouse, N. I. and Vukusic, P. (2009). A protean palette: colour materials and mixing in birds and butterflies. *J. R. Soc. Interface* **6,** S221-S231.

Stavenga, D. G. (2014). Thin film and multilayer optics cause structural colors of many insects and birds. *Mat. Today Proc.* **1S,** 109-121.

Stavenga, D. G., Leertouwer, H. L., Osorio, D. C. and Wilts, B. D. (2015). High refractive index of melanin in shiny occipital feathers of a bird of paradise. *Light Sci. Appl.* **4,** e243.

Stavenga, D. G., Leertouwer, H. L., Marshall, N. J. and Osorio, D. (2010). Dramatic colour changes in a bird of paradise caused by uniquely structured breast feather barbules. *Proc. R. Soc. B* **278,** 2098-2104.

Stavenga, D. G., Leertouwer, H. L., Pirih, P. and Wehling, M. F. (2009). Imaging scatterometry of butterfly wing scales. *Opt. Exp.* **17,** 193-202.

Stavenga, D. G., Tinbergen, J., Leertouwer, H. L. and Wilts, B. D. (2011). Kingfisher feathers - colouration by pigments, spongy nanostructures and thin films. *J. Exp. Biol.* **214,** 3960-3967.

Stavenga, D. G., van der Kooi, C. J. and Wilts, B. D. (2017). Structural coloured feathers of mallards act by simple multilayer photonics. *J. R. Soc. Interface* **14,** 10.1098/rsif.2017.0407.

Tinbergen, J., Wilts, B. D. and Stavenga, D. G. (2013). Spectral tuning of Amazon parrot feather coloration by psittacofulvin pigments and spongy structures. *J. Exp. Biol.* **216,** 4358-4364.

Vigneron, J. P., Colomer, J., Rassart, M., Ingram, A. L. and Lousse, V. (2006). Structural origin of the colored reflections from the black-billed magpie feathers. *Phys. Rev. E* **73,** 021914.

Vukusic, P. and Stavenga, D. G. (2009). Physical methods for investigating structural colours in biological systems. *J. R. Soc. Interface* **6:Suppl 2,** S133-148.

Wilts, B. D., Leertouwer, H. L. and Stavenga, D. G. (2009). Imaging scatterometry and microspectrophotometry of lycaenid butterfly wing scales with perforated multilayers. *J. R. Soc. Interface* **6,** S185-S192.

Wilts, B. D., Michielsen, K., De Raedt, H. and Stavenga, D. G. (2014). Sparkling feather reflections of a bird-of-paradise explained by finite-difference time-domain modeling. *Proc. Natl. Acad. Sci. U. S. A.* **111,** 4363-4368.

Xiao, M., Dhinojwala, A. and Shawkey, M. (2014). Nanostructural basis of rainbow-like iridescence in common bronzewing Phaps chalcoptera feathers. *Opt. Express* **22,** 14625-14636.

Yoshioka, S., Nakamura, E. and Kinoshita, S. (2007). Origin of two-color iridescence in rock dove's feather. *J. Phys. Soc. Japan* **76,** 013801

Figures

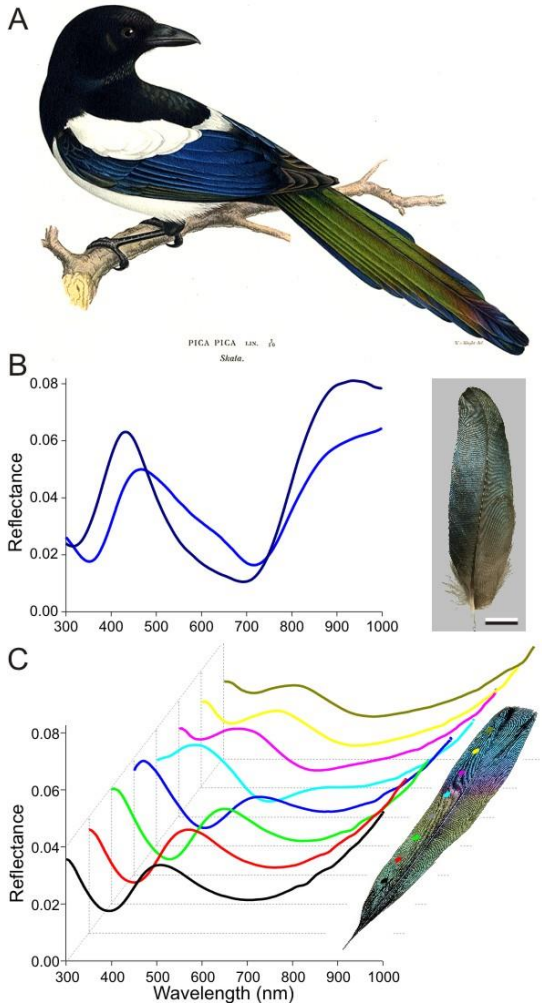

Fig. 1. The common magpie, *Pica pica*, and its variously coloured plumage. (A) Drawing by Wilhelm von Wright (1810 - 1887; from the public domain). (B) Reflectance spectra of different areas of a secondary feather measured with an integrating sphere. Inset: a blue secondary feather; scale bar: 1 cm. (C) Reflectance spectra of different areas of a tail feather. Inset: the tail feather with the measured areas, indicated by coloured dots corresponding with the colours of the reflectance spectra. Distance between the coloured dots: 1 cm.

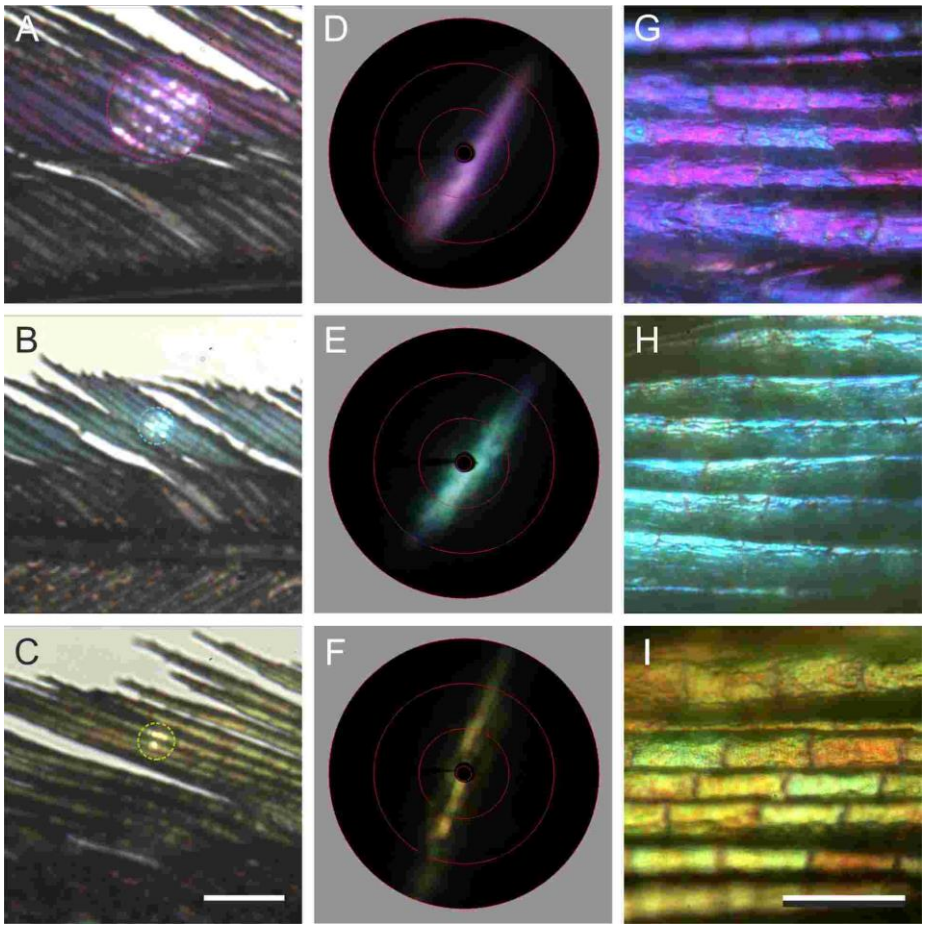

Fig. 2. Scatterometry of differently coloured barbules of a magpie tail feather. (A-C) Differently coloured feather areas, locally illuminated at a spot marked by a dashed circle. (D-F) Scatterograms created by the spot illuminations of A-C. The red circles indicate angular directions of 5º, 30º, 60º, and 90º. (G-I) Epi-illumination light micrographs of a purple, blue, and green feather area, respectively, showing the slightly varying colour of the barbule cells. Scale bars, A-C: 50 µm, D-F: 100 µm.

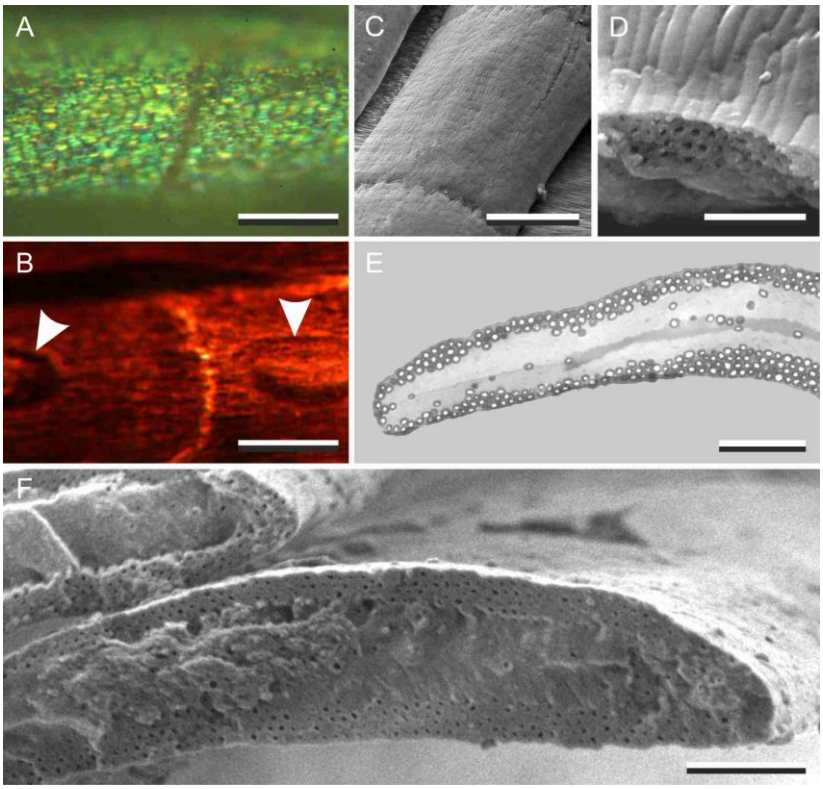

Fig. 3. Barbule anatomy. (A) Epi-illumination light micrograph of a barbule in oil immersion, showing the somewhat irregular organization of the melanosomes. (B) Transmitted light micrograph of an immersed barbule, revealing a dense melanin pigmentation; arrowheads: cell nuclei. (C) Scanning electron micrograph (SEM), showing the curved and corrugated surface of the barbule cells with tightly packed melanosomes. (D) SEM of a sectioned barbule, showing the hollow melanosomes stacked in two to three layers. (E) Transmission electron micrograph of a barbule with melanosome stacks on both the upper and under side. (F) SEM of sectioned feather barbules, showing the hollow melanosome layers on both the upper and lower sides of the barbules. Scale bars, A-C: 10 µm; D: 1 µm; E, F: 2 µm.

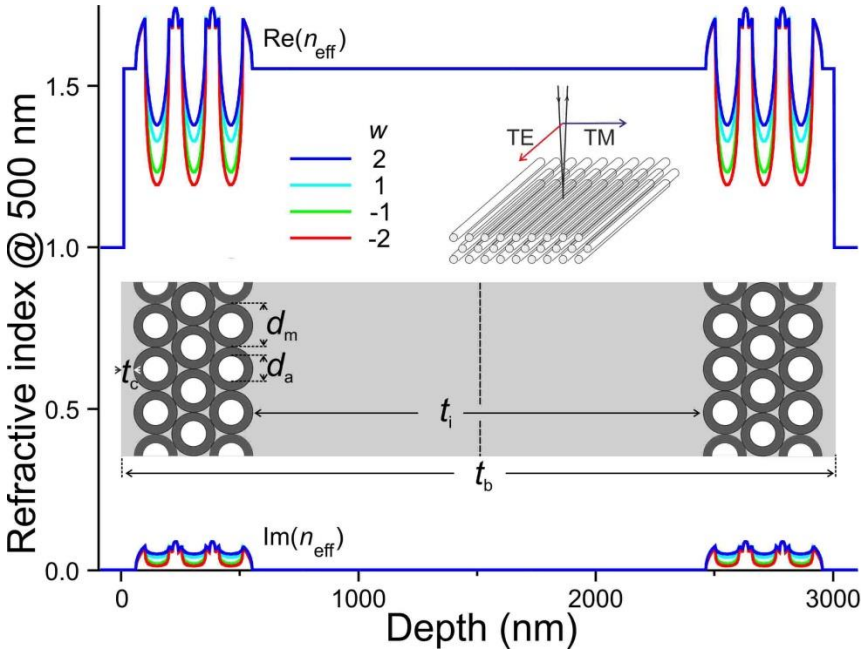

Fig. 4. Refractive index profiles and diagram of a magpie barbule. Upper inset: melanin rodlets (about) normally illuminated. With the plane of light incidence perpendicular to the melanosome stack, the electric vectors of TE- and TM-polarised light are parallel and perpendicular to the rodlets, respectively. Lower inset: Cross-section of a barbule showing stacks with three layers of close-packed, air-filled melanosomes embedded in keratin near both sides of the barbule. The total barbule thickness is t_b = 3000 nm, with an epicuticle thickness t_c = 50 nm, melanosome diameter d_m = 180 nm, air hole diameter d_a = 100 nm, and thickness of the intermediate keratin layer t_i = 1916 nm. The profiles of the real and imaginary components of the effective refractive index, n_{eff}, for 500 nm light were calculated with Eq. 1 for w = -2, -1, 1, and 2.

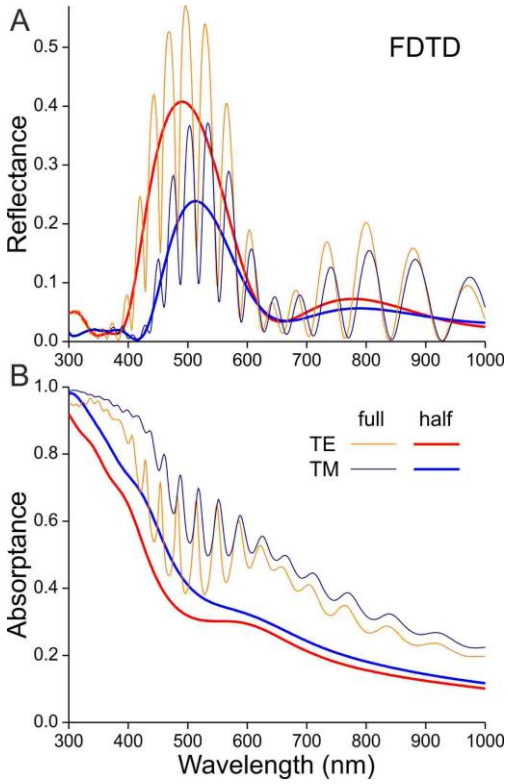

Fig. 5. FDTD optical modelling of a magpie barbule. (A) Reflectance spectra of the full barbule of Figure 4 as well of only half the barbule, for normally incident TE- and TM-polarised light. (B) The corresponding absorptance spectra.

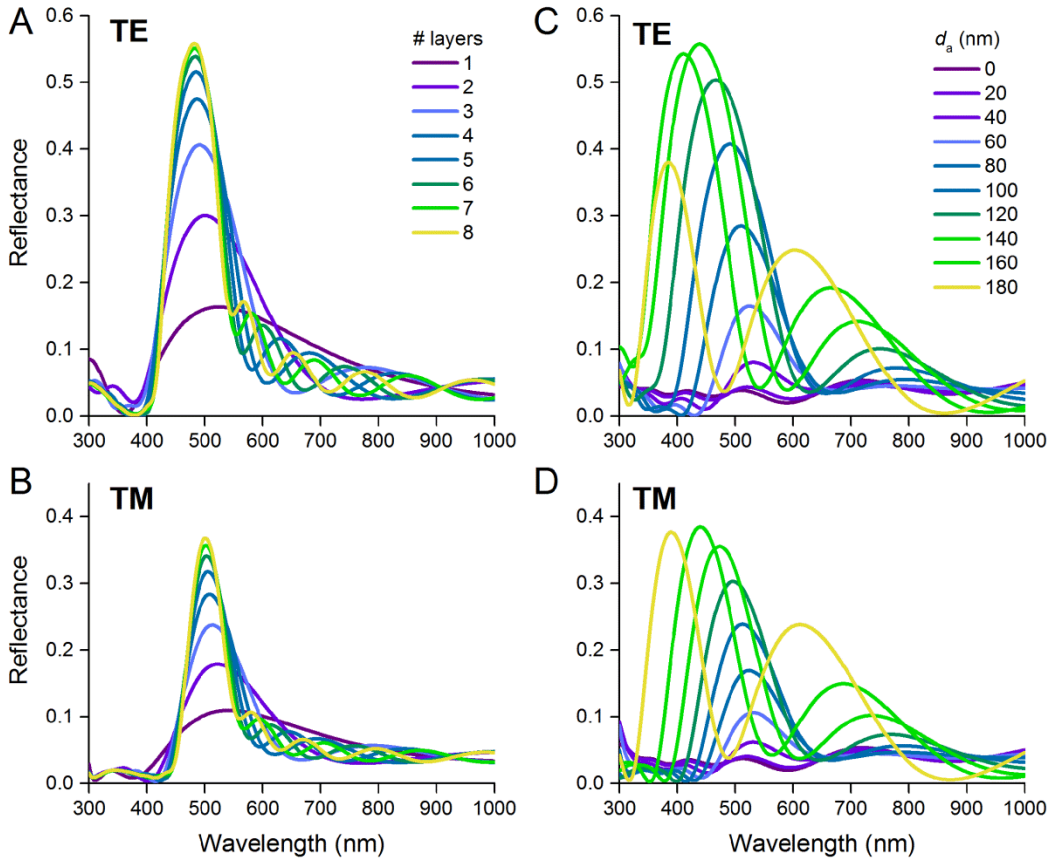

Fig. 6. Dependence of the reflectance of a half barbule on the number of melanosome layers and air hole diameter calculated with the FDTD method. (A, B) Reflectance spectra for TE- and TM-polarised light for 1 to 8 layers of melanosomes with outer diameter d_m = 180 nm and air hole diameter d_a = 100 nm. (C, D) Reflectance spectra for normally incident TE- and TM-polarised light for N = 3 layers of melanosomes with diameter d_m = 180 nm and air hole diameter d_a varying from 0 to 180 nm.

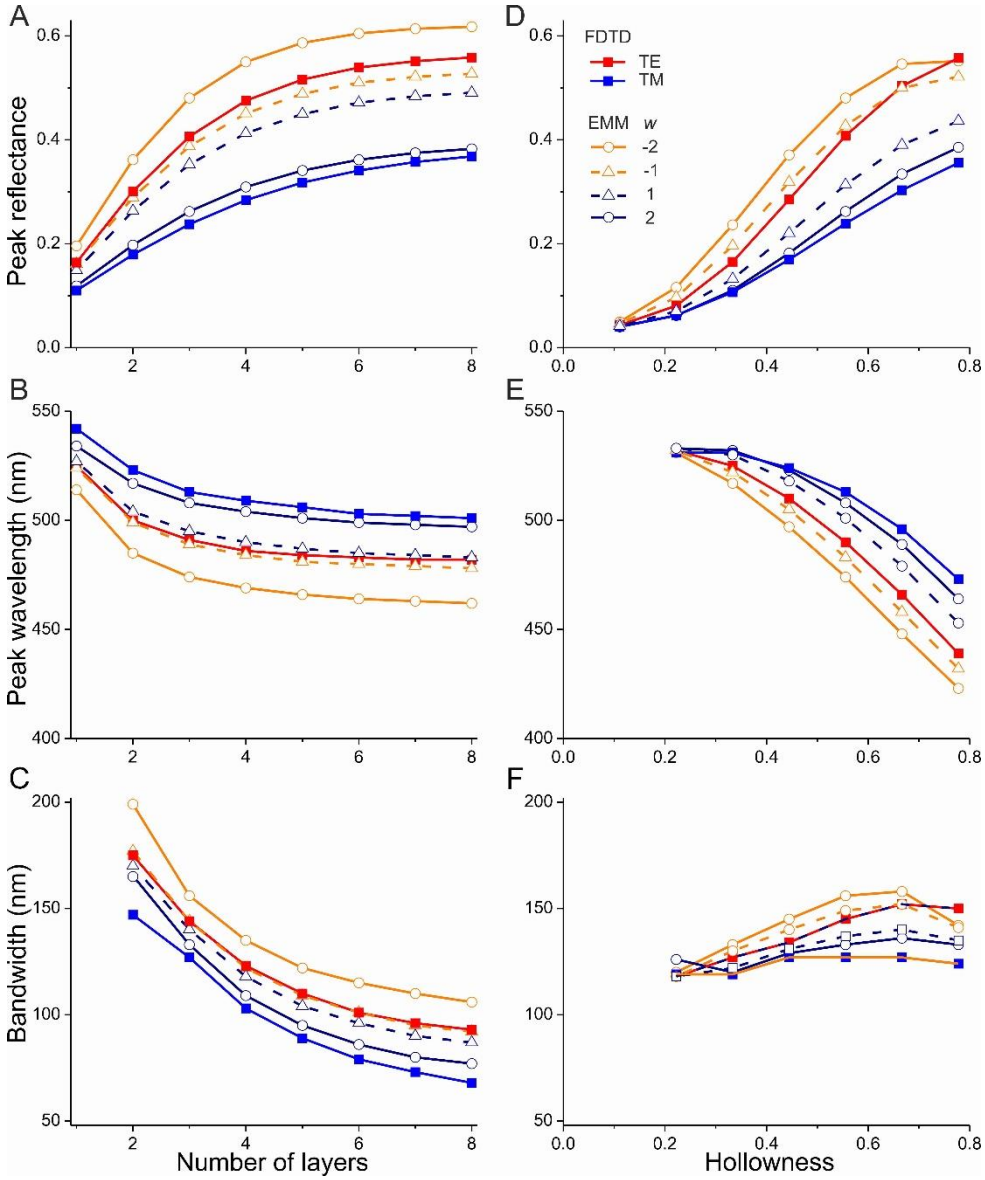

Fig. 7. Comparison of reflectance spectra characteristics calculated with the finite-difference time-domain (FDTD) and effective medium multilayer (EMM) methods for normally incident TE- and TM-polarised light. (A-C) Peak reflectance, peak wavelength and spectral bandwith of a half barbule with melanosome diameter d_m = 180 nm and air core diameter d_a = 100 nm as a function of the number of melanosome layers. (D-F) Peak reflectance, peak wavelength and spectral bandwith of a half barbule with three layers of melanosomes with diameter d_m = 180 nm as a function of the hollowness $h = d_m/d_a$.

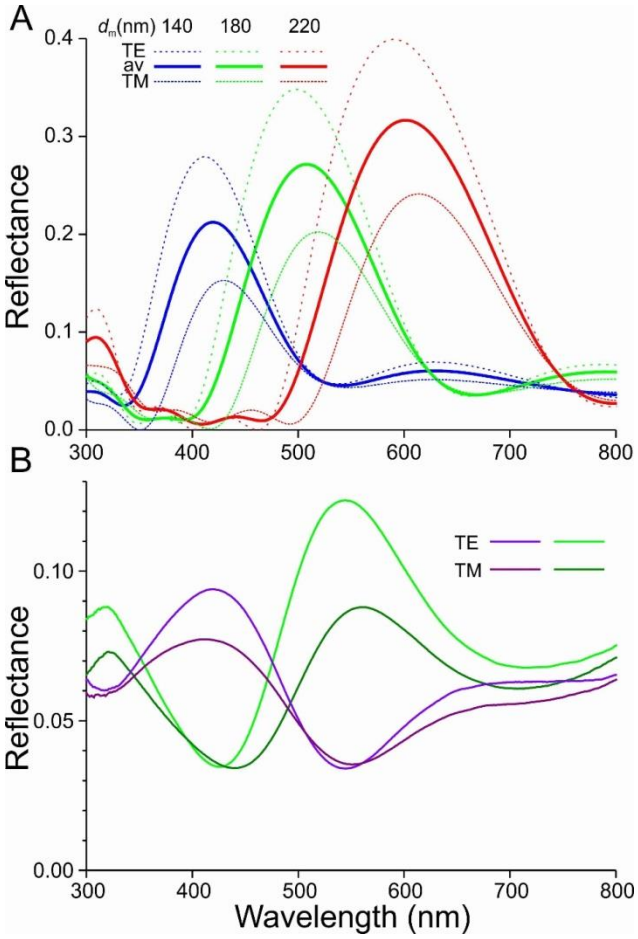

Fig. 8. Reflectance spectra for normally incident TE- and TM-polarised light. (A) Spectra calculated with the multilayer method for (half) a barbule with three layers of melanosomes with different diameter of the melanosomes, assuming a constant hollowness of h = 0.5; av: average of the TE- and TM-spectra. (B) TE- and TM-spectra measured from the purple and green areas of the tail feather of Fig. 1C.

Supplementary Material

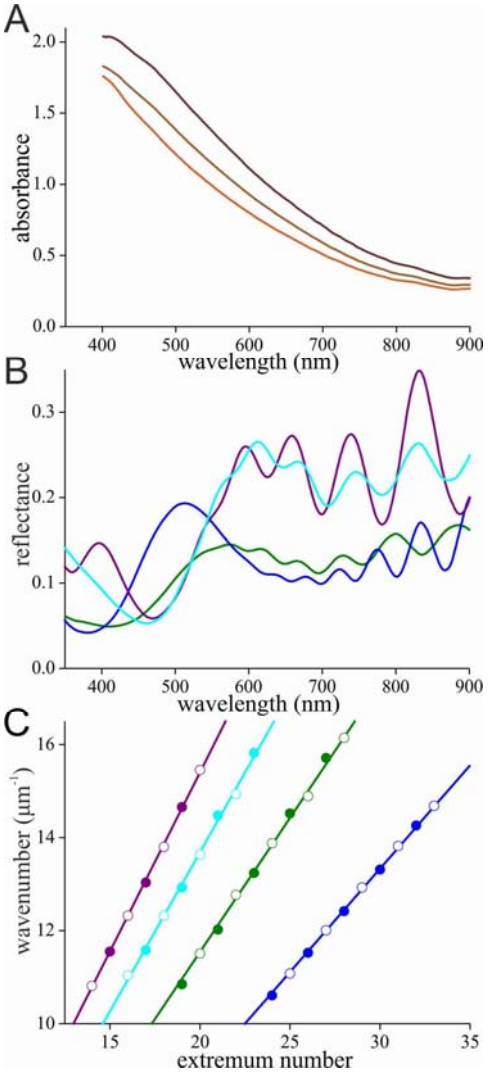

Fig. S1. Optical characteristics of single barbule cells. (A) Absorbance spectra of three different barbules immersed in immersion oil measured with a microspectrophotometer (MSP; area cross section ~10 µm). (B) MSP reflectance spectra of four different barbules in air, showing oscillations. (C) Wave numbers calculated with the wavelength values of the oscillation minima (open circles) and maxima (closed circles) > 600 nm of the four spectra of panel A. The fitted linear functions yielded the local barbule thickness: 2.0 µm (purple data), 2.3 µm (cyan), 2.7 µm (green), and 3.5 µm (blue).

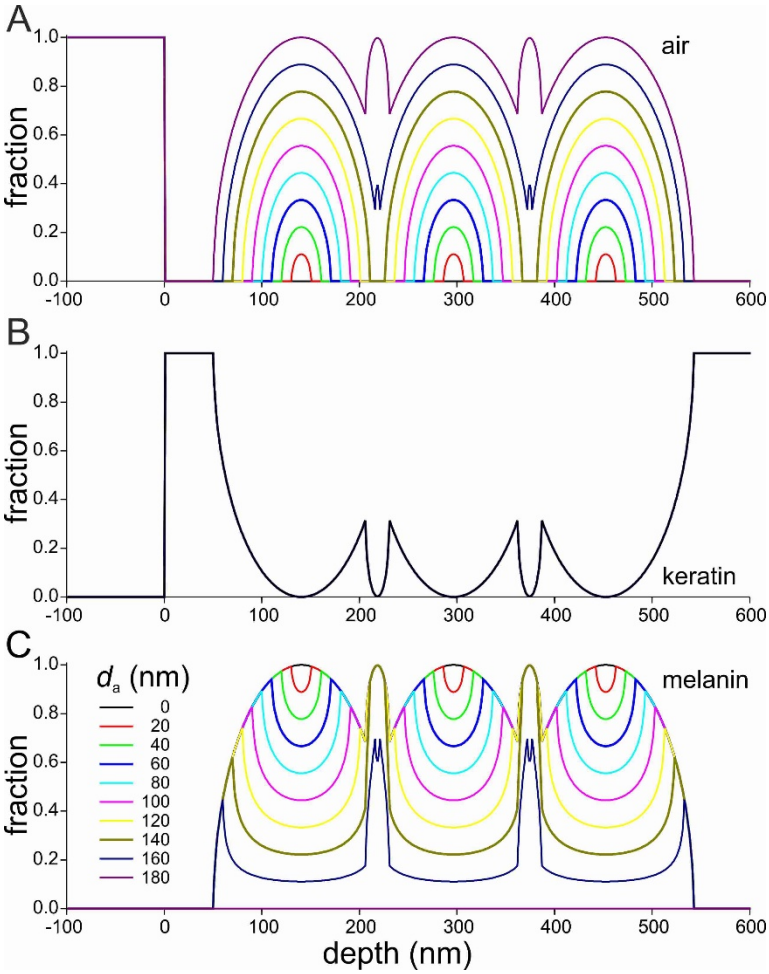

Fig. S2. The fractions of air (A), keratin (B), and melanin (C) as a function of depth for three layers of close-packed melanosomes with diameter d_m = 180 nm and variously sized air holes with diameter d_a.

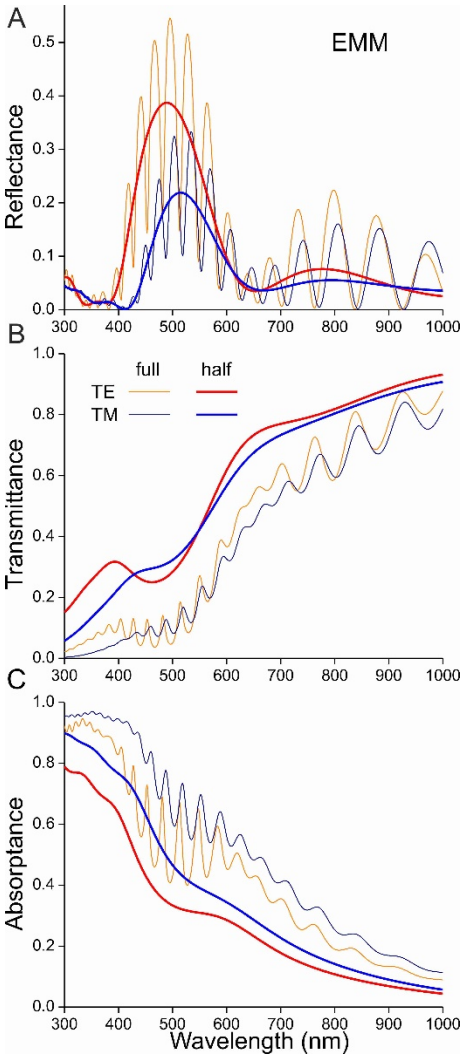

Fig. S3. Reflectance (A), transmittance (B), and absorptance (C) spectra of the full barbule of Fig. 4 as well only half the barbule, for normally incident TE- and TM-polarised light, calculated with the transfer-matrix formalism for effective medium multilayers (EMM), using the refractive index profiles of Fig. 4 for w = -2 and 2, respectively.

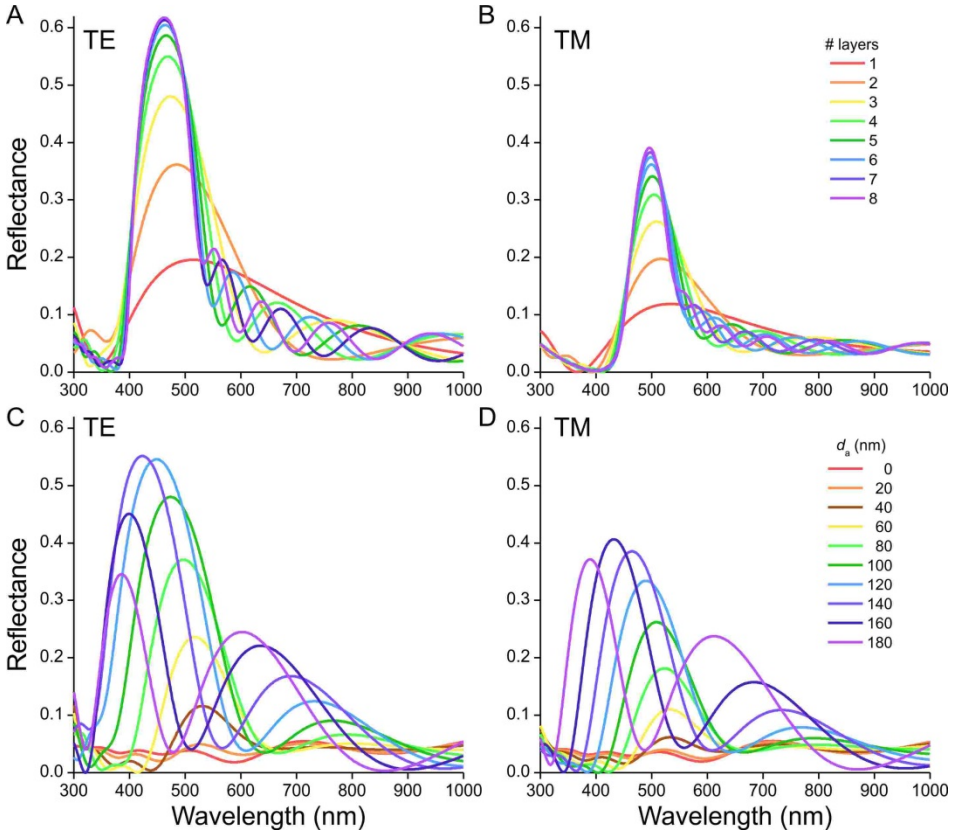

Fig. S4. Dependence of the reflectance of a half barbule on the number of melanosome layers and air core diameter calculated with the transfer-matrix formalism for multilayers. (A, B) Reflectance spectra for 1 to 8 layers of melanosomes with diameter d_m = 180 nm and air hole diameter d_a = 100 nm, using the refractive index profiles of Fig. 4 for w = -2 and 2 for TE- and TM-polarised light, respectively. (C, D) Reflectance spectra for TE- and TM-polarised light for three layers of melanosomes with diameter d_m = 180 nm and air hole diameters of 0 to 180 nm.

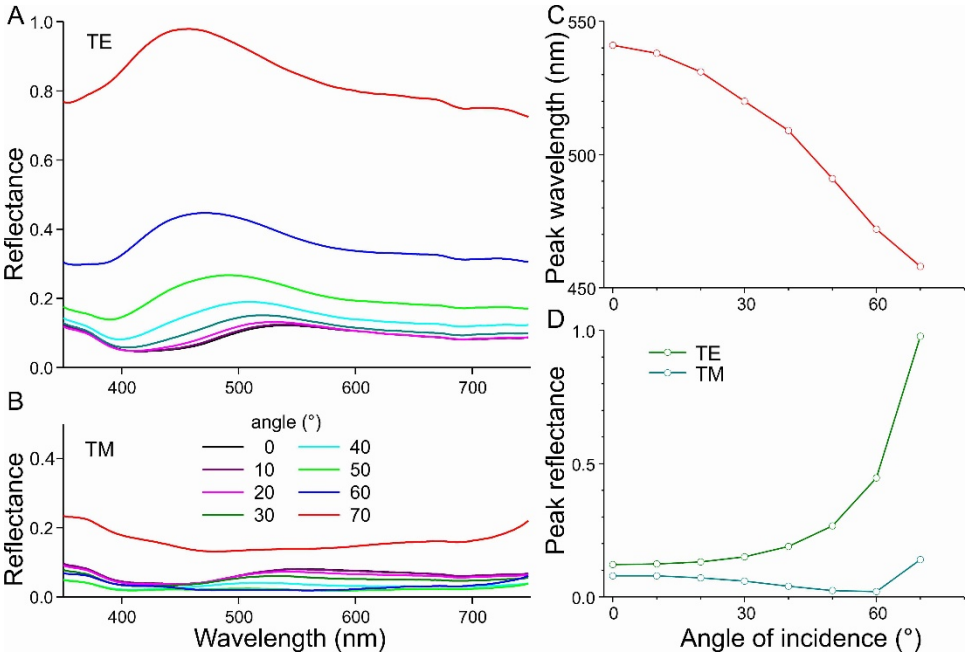

Fig. S5. Angle dependence of the reflectance of TE- and TM-polarised light for the green area of the magpie feather in Fig. 1C. (A) Reflectance spectra of TE-polarised light for angles of light incidence 0º to 70º. (B) Reflectance spectra of TE-polarised light. (C) Peak wavelength of the reflectance spectra of (A) as a function of the angle of light incidence. (D) Reflectance values at the peak wavelengths in (C) for TE- and TM-polarised light.

Supplementary Material

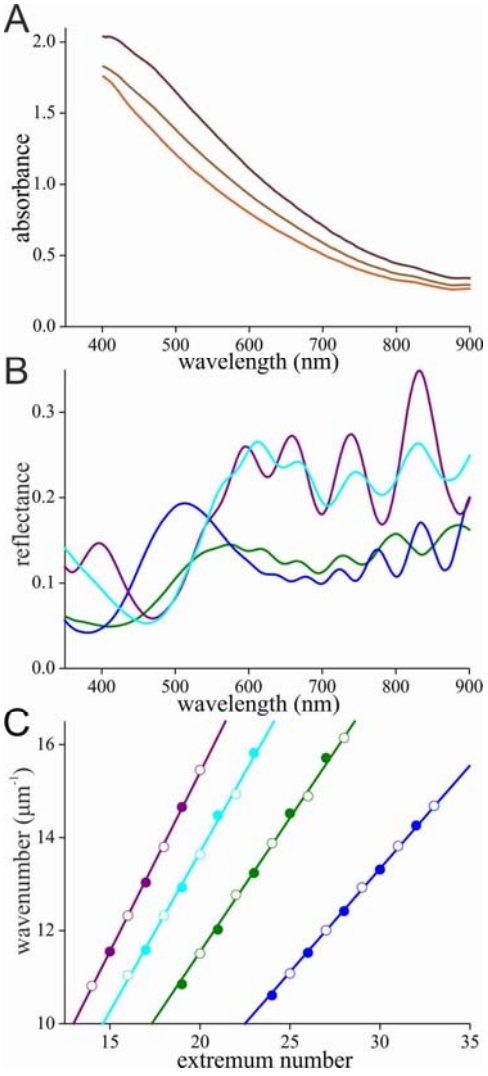

Fig. S1. Optical characteristics of single barbule cells. (A) Absorbance spectra of three different barbules immersed in immersion oil measured with a microspectrophotometer (MSP; area cross section ~10 µm). (B) MSP reflectance spectra of four different barbules in air, showing oscillations. (C) Wave numbers calculated with the wavelength values of the oscillation minima (open circles) and maxima (closed circles) > 600 nm of the four spectra of panel A. The fitted linear functions yielded the local barbule thickness: 2.0 µm (purple data), 2.3 µm (cyan), 2.7 µm (green), and 3.5 µm (blue).

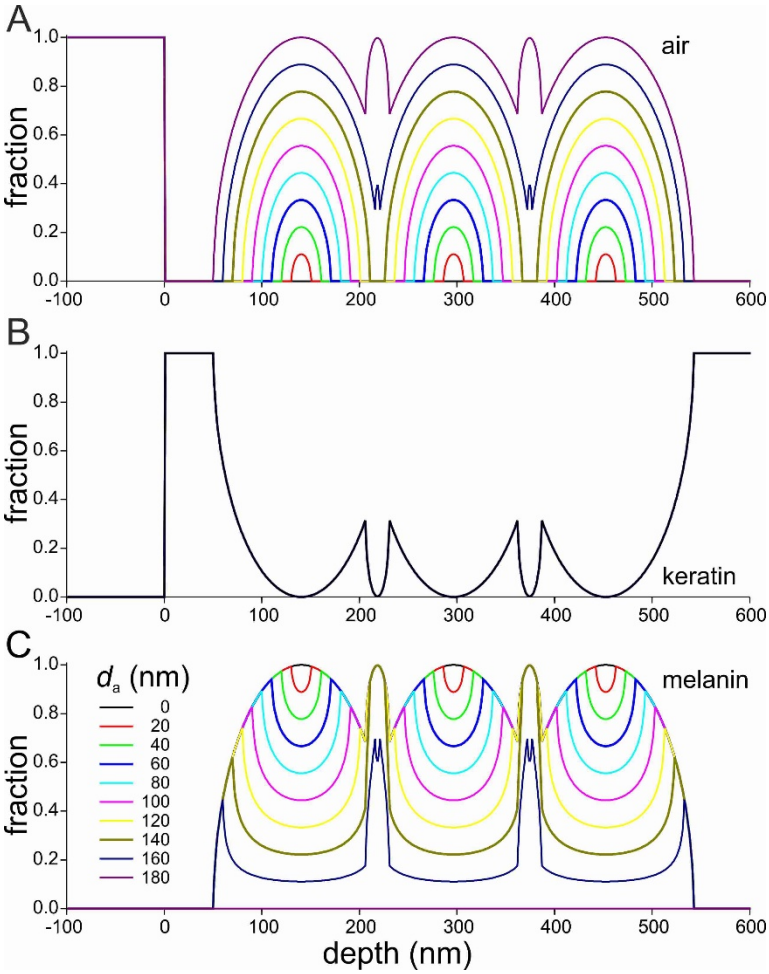

Fig. S2. The fractions of air (A), keratin (B), and melanin (C) as a function of depth for three layers of close-packed melanosomes with diameter d_m = 180 nm and variously sized air holes with diameter d_a.

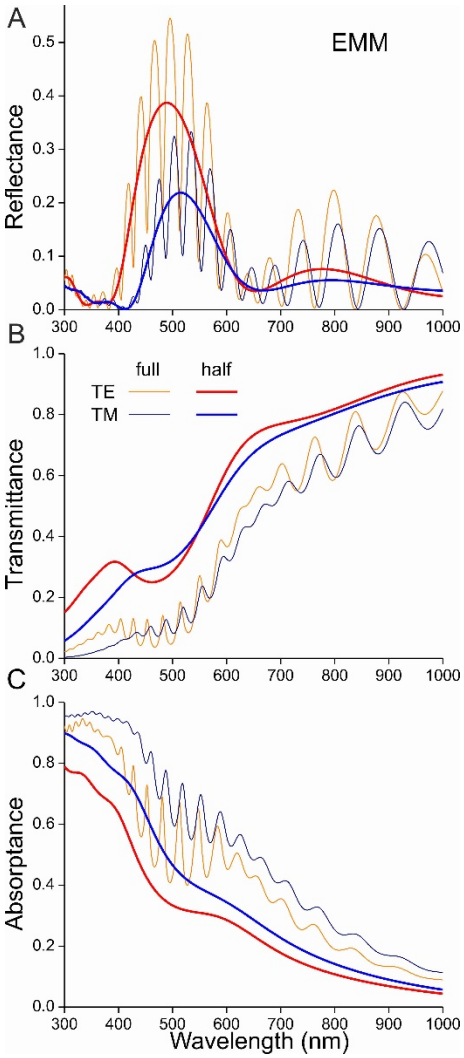

Fig. S3. Reflectance (A), transmittance (B), and absorptance (C) spectra of the full barbule of Fig. 4 as well only half the barbule, for normally incident TE- and TM-polarised light, calculated with the transfer-matrix formalism for effective medium multilayers (EMM), using the refractive index profiles of Fig. 4 for w = -2 and 2, respectively.

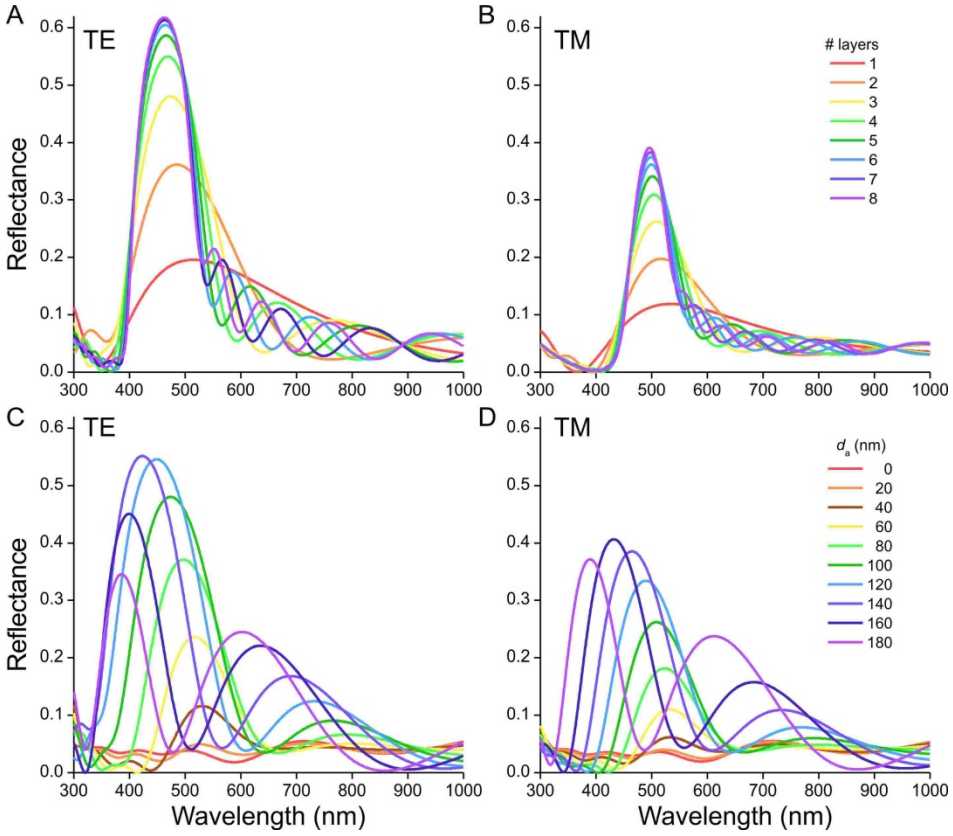

Fig. S4. Dependence of the reflectance of a half barbule on the number of melanosome layers and air core diameter calculated with the transfer-matrix formalism for multilayers. (A, B) Reflectance spectra for 1 to 8 layers of melanosomes with diameter d_m = 180 nm and air hole diameter d_a = 100 nm, using the refractive index profiles of Fig. 4 for w = -2 and 2 for TE- and TM-polarised light, respectively. (C, D) Reflectance spectra for TE- and TM-polarised light for three layers of melanosomes with diameter d_m = 180 nm and air hole diameters of 0 to 180 nm.

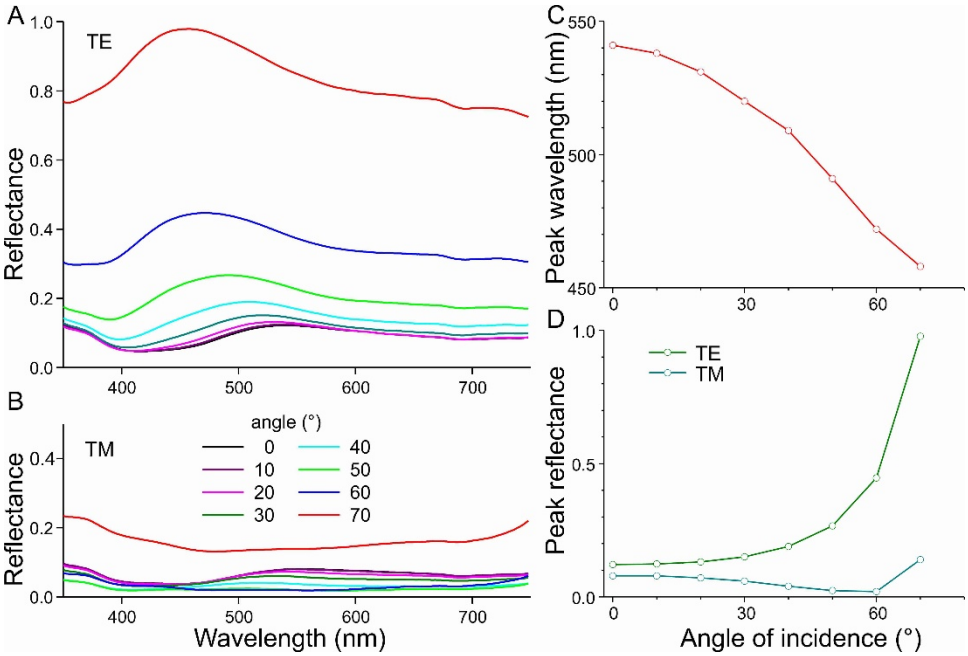

Fig. S5. Angle dependence of the reflectance of TE- and TM-polarised light for the green area of the magpie feather in Fig. 1C. (A) Reflectance spectra of TE-polarised light for angles of light incidence 0º to 70º. (B) Reflectance spectra of TE-polarised light. (C) Peak wavelength of the reflectance spectra of (A) as a function of the angle of light incidence. (D) Reflectance values at the peak wavelengths in (C) for TE- and TM-polarised light.